Radiation Measurements 136 (2020) 106426

Contents lists available at ScienceDirect

Radiation Measurements

journal homepage: www.elsevier.com/locate/radmeas

Use of portable gamma spectrometers for triage monitoring following the intake of conventional and novel radionuclides

Siria Medici [a,b], Pierre Carbonez [a,c], Jérôme Damet [b,c], François Bochud [b], Andreas Pitzschke [b,*]

[a] European Organization for Nuclear Research (CERN), Geneva, Switzerland
[b] Institute of Radiation Physics, Lausanne University Hospital Center, Switzerland
[c] Department of Radiology, University of Otago, Christchurch, New Zealand

ARTICLE INFO

Keywords:
Intake of radionuclides
Portable gamma spectrometers
Novel radionuclides
Triage monitoring
Instrument characterisation

ABSTRACT

Current internal dosimetry monitoring programmes generally feature periodic measurements that are defined for the most commonly-encountered radionuclides. These programmes are not directly applicable to research centres that produce novel and short-lived radionuclides which are then used for the manufacture of radiopharmaceuticals, such as the CERN-MEDICIS facility hosted at CERN. This work presents an in vivo internal dosimetry programme based on the concept of triage monitoring. The programme allows to comply with the annual committed effective dose limit of E_{50} = 1 mSv by performing rapid gamma-spectroscopy screening measurements. Two portable spectrometers (HPGe- and NaI-based) were characterised using two different phantoms: a simplified model of the human torso and an anthropomorphic phantom allowing for customised source-filling geometries. The efficiencies of the spectrometers were determined using both phantoms and the minimum detectable activities were computed as a function of the measuring time for a selection of 21 among novel and conventional radionuclides. The minimum detectable activity was then used to calculate the minimum committed effective dose associated to each measurement for a realistic intake scenario. For a single screening measurement of 30 s performed at the end of the working day, the minimum detectable committed effective dose resulting from a radionuclide inhalation ranged between few μSv and hundreds of μSv for the majority of the considered radionuclides. The suggested approach allows to set up pragmatic in vivo measurements to monitor the workers' internal contamination in research centres and industries where unsealed conventional and/or novel radionuclides may be handled.

1. Introduction

The aim of internal dosimetry monitoring programmes is to protect workers against the risk of intake of radionuclides and ensure that the protection complies with legal requirements (ISO, 2006). These are set by national regulatory authorities based on guidance provided by international standards (IAEA, 1999; EC, 2018; ISO, 2011). Individual in vivo monitoring aims to retrospectively determine the committed effective dose E_{50} by quantifying the activity retained in the whole body or in a considered body region after an intake. The original intake activity is then calculated with the help of retention functions obtained by biokinetic models and the E_{50} is determined by applying committed effective dose coefficients. In vivo monitoring approaches for the quantification of internal exposure are described in numerous international standards and guidelines (ISO, 2006, 2016; ICRU, 2003; Castellani et al., 2013). Dose estimations in the field of internal dosimetry are prone to large uncertainties and international standards permit committed effective dose underestimations by up to a factor of 3 (ISO, 2006). The monitoring is usually performed routinely by defining a particular measuring technique and a time interval between controls and is restricted to commonly-encountered radionuclides.

The European Organization for Nuclear Research (CERN) is currently reviewing its internal dosimetry monitoring programme, in particular following the commissioning of the CERN-MEDICIS facility that produces novel radionuclides for medical applications, such as theranostics. The radionuclides are then shipped to the partner centres and used in preclinical and clinical trials. Due to the short half-life of the produced unsealed radionuclides and the rapid turnover of the workers, routine in vivo measurements are impractical for intervals longer than a few days (ISO, 2016). Thus, a programme for the monitoring of uncommon radionuclides through screening measurements was developed. The programme is inspired by the Swiss radiation protection regulation (FOPH, 2017a,b) that is based on the concept of triage monitoring presented in the ISO 16637 standard (ISO, 2016) and aims

* Corresponding author.
E-mail address: andreas.pitzschke@chuv.ch (A. Pitzschke).

https://doi.org/10.1016/j.radmeas.2020.106426
Received 22 January 2020; Received in revised form 29 April 2020; Accepted 19 June 2020
Available online 27 June 2020

to ensure the detection of intakes leading to an annual $E_{50} > 1$ mSv. Screening measurements do not aim to precisely quantify an intake, but rather to trigger further investigation if a specific threshold is exceeded, such as in vivo or in vitro incorporation measurements (ISO, 2016; EC, 2018).

A previous work already confirmed the feasibility to perform in vivo screening measurements using conventional radiation protection instruments, such as dose rate meters and contamination monitors (Medici et al., 2019). However, the considered conventional instruments do not allow for radionuclide identification (i.e. the potentially incorporated radionuclide has to be known prior to the measurement) nor for the monitoring of unknown radionuclide mixtures (such as radioactive impurities in the main product). Therefore, it has been decided to extend the existing approach to two portable gamma-spectrometers that address these limitations.

The use of portable spectrometers for in vivo measurements has already been described in the literature (Galeev et al., 2016; Dewji et al., 2013; Ha and Kim, 2016; Muikku and Rahola, 2007; Youngman, 2008; Kramer et al., 2005; Terranova et al., 2010). These studies generally determine the instruments performance in the case of radiological emergencies (presenting higher dose constraints than the ones of occupational monitoring) and focus on the monitoring of commonly-encountered radionuclides. However, to our knowledge, the monitoring of novel radioisotopes is yet to be undertaken.

In this work, we characterised two portable spectrometers using two different phantoms and we determined their performances for the in vivo internal monitoring of a selection of novel and conventional radionuclides. The minimum detectable activity is provided as a function of the acquisition time and the minimum detectable committed effective dose associated to a screening measurement is calculated for typical intake scenarios.

2. Materials and methods

2.1. Instruments and phantoms

Two portable spectrometers were characterised: a HPGe-based Falcon 5000 (Canberra Industries Inc., USA) and a 2 ”× 2” cylindrical NaI(Tl) detector (SCIONIX, NL). The NaI(Tl) detector was coupled to an Osprey multi-channel analyser tube base (Canberra Industries Inc., USA).

Two different phantoms were used for the characterisation of the spectrometers. The first consists in a cylindrical plastic bucket (30 cm of diameter, 36 cm of height, 2 mm of thickness) filled with water. This simplified and easily reproducible phantom mimics a human torso and has already been used for the characterisation of conventional radiation protection instruments (Medici et al., 2019). The reference sources (^{133}Ba, ^{137}Cs, ^{60}Co, ^{152}Eu) allowed to cover a wide photon energy range (~80–1400 keV) and were positioned at the centre of the phantom. The sources were all in liquid form and were conditioned in 20 ml glass or polyethylene vials. Their activity ranged between 100 and 400 kBq at the time of the calibration and was certified by the Radiometrology Group of the Institute of Radiation Physics in Lausanne, which is designated by the Federal Institute of Metrology (METAS) as the primary standard laboratory for the unit of activity (Bq) in Switzerland. The calibration was performed in a contact geometry, as shown in Fig. 1.

The second phantom used for the characterisation of the spectrometers is the so-called IGOR phantom manufactured by the Research Institute of Sea Transport Hygiene in St. Petersburg (Kovtun et al., 2000). The IGOR phantom is recommended by the Swiss Expert Group for Dosimetry (SEGD) for the calibration of whole body and lung counters (KSR, 2001a,b). It consists of polyethylene blocks (density = 0.95 g/cm^3) that can be assembled to reproduce 6 different configurations (from P1 to P6). In the present study, the P4 configuration (standard adult, 70 kg) was considered and the phantom was assembled in a standing geometry. The blocks come in two dimensions (165 × 110 × 55 mm^3 for 0.88 kg and 165 × 110 × 25 mm^3 for 0.40 kg) and each block is provided with two cylindrical holes that allow the insertion of two pencil-like sources (163 mm length, 6 mm diameter). The reference sources used for the characterisation of the spectrometers with the IGOR phantom (^{133}Ba, ^{137}Cs, ^{60}Co, ^{152}Eu) were manufactured by the Radiometrology Group of the Institute of Radiation Physics in Lausanne.

Fig. 1. Torso phantom showing the Falcon 5000 positioning during calibration. The arrow indicates the support allowing the placement of the reference sources inside the phantom.

The calibration of the spectrometers was performed in a contact geometry and two source filling geometries were tested. The thorax filling geometry (cf. Figs. 2(a) and 2(b)) was used to simulate a radionuclide retention in the lungs, while the abdomen filling geometry (cf. Figs. 2(c) and 2(d)) aimed to reproduce a radionuclide retention in the alimentary tract. For each filling geometry, two different source distributions were tested: shallow and deep. For both geometries, 16 sources were used. The thorax-deep configuration (Fig. 2(a)) is the calibration geometry suggested by the SEGD for screening measurements to be performed at the level of the thorax (KSR, 2001b). We used the same number of sources and relative position within the phantom to define the source distribution in the case of the abdomen filling (abdomen-deep, Fig. 2(c)), for which no information was provided in the SEGD report. We also chose an alternative source filling configuration, where sources were less deep in the phantom, as we considered it to be more anatomically realistic (abdomen-shallow, Fig. 2(d)). The same approach was thus applied to the thorax filling for the sake of consistency (thorax-shallow, Fig. 2(b)). In the shallow configuration, the average source depth was 5.5 cm for the thorax filling and 11 cm for the abdomen filling, while in the deep configuration the average source depth was 11 cm for the thorax filling and 16.5 cm for the abdomen filling. The total activity contained in the IGOR phantom ranged between 1.8 and 34 kBq at the time of the calibration.

2.2. Efficiency calibration

For the calibration of the spectrometers, the reference sources (^{133}Ba, ^{137}Cs, ^{60}Co, ^{152}Eu) were placed one after the other in the phantoms and spectra were acquired over several hours in order to reduce the errors associated to counting statistics. The measurements took place in a standard background environment (ambient dose rate between 80 and 120 nSv/h) and no shielding was used. Spectral analysis was performed using Genie 2000 Gamma Analysis Software, ver. 3.3 (Canberra Industries Inc., USA). The calibration spectra were analysed after subtraction of a background spectrum, acquired with the phantoms in the absence of sources. For each filling geometry (thorax or abdomen) and source distribution (deep or shallow), the spectral analysis results of the four reference sources were combined to establish the detector efficiency in the considered configuration. For the Falcon 5000, the efficiency was directly calculated by the Genie 2000 software and used to assess the coefficients of the efficiency curve fit. Concerning

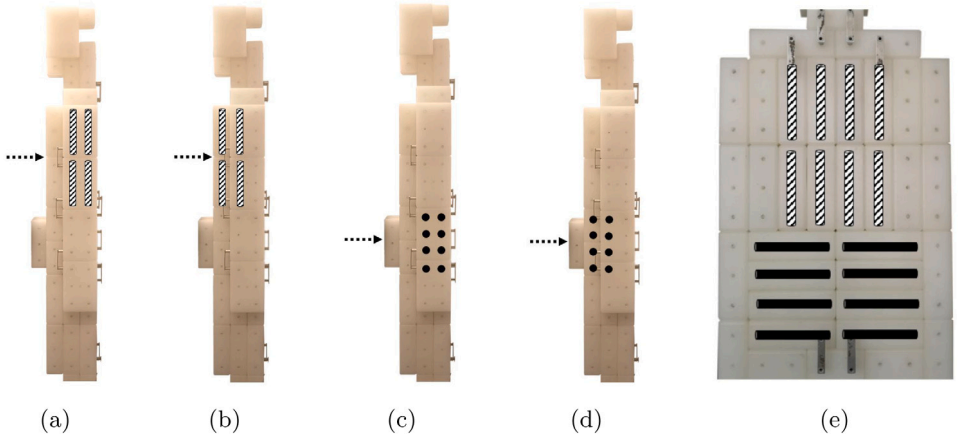

Fig. 2. IGOR phantom showing the positioning of the instruments during calibration (dashed arrow). The source positioning is depicted with a stripe pattern for the thorax filling geometry (deep and shallow configuration) (a, b) and in black for the abdomen filling geometry (deep and shallow configuration) (c, d). The source positioning as seen from the back of the phantom is also shown for illustration purposes (e). It should be noted that only one filling geometry (thorax or abdomen) was used at a time in the IGOR phantom.

the NaI(Tl) detector, the efficiency ε (in cps/Bq) was calculated from the net peak area provided by the Genie 2000 software using Eq. (1):

$$\varepsilon = \frac{N}{t \cdot A \cdot p_{\%}} \tag{1}$$

where N is the net peak area (in counts), t is the acquisition time (in s), A is the source activity in the phantom (in Bq) and $p_{\%}$ is the photon emission probability of the considered emission line. The energy-efficiency pairs were then manually entered in Genie 2000 to calculate the coefficients of the efficiency curve fit.

For both spectrometers, the efficiency curves were obtained using one of the two polynomial expressions given in Eq. (2), available in the Genie 2000 software.

$$ln(\varepsilon) = \sum_{i=0}^{n} x_i \cdot ln(E)^i \tag{2a}$$

$$log(\varepsilon) = \sum_{i=0}^{n} x_i \cdot (E)^{1-i} \tag{2b}$$

where x_i are the coefficients of the polynomial, ln is the natural logarithm, log is the common logarithm and E is the energy of the considered gamma line emission (in keV). The selected polynomial expression is the one showing the lowest mean absolute percent difference between the fitted efficiency curve and the experimental energy-efficiency pairs. We chose the highest order of the polynomial that did not lead to unphysical features in the efficiency curves due to overfitting.

Table 1
Radionuclides of interest considered in this study, along with their half-lives, fields of application and characteristics. The half-lives correspond to the ones reported in ICRP Publication 107 (m = minutes, h = hours, d = days, y = years) (ICRP, 2008).

Radionuclide	Half-life	Field	Description
^{54}Mn	312.12 d	Ind.	activation product
^{60}Co	5.2713 y	Ind.	activation product[a]
^{133}Ba	10.52 y	Ind.	activation product
^{137}Cs	30.1671 y	Ind.	activation product[a]
^{152}Eu	13.537 y	Ind.	activation product
^{131}I	8.02070 d	Ind./Med.	β therapy, activation product[a]
^{18}F	109.77 m	Med.	diagnostics (PET)
^{47}Sc	3.3492 d	Med.	β therapy and diagnostics (SPECT)
^{64}Cu	12.700 h	Med.	β therapy and diagnostics (PET)
^{67}Cu	61.83 h	Med.	β therapy and diagnostics (SPECT)
^{68}Ga	67.71 m	Med.	diagnostics (PET)
^{76}As	1.0778 d	Med.	β therapy
^{77}As	38.83 h	Med.	β therapy
^{99m}Tc	6.015 h	Med.	diagnostics (SPECT)
^{149}Tb	4.118 h	Med.	α therapy and diagnostics (PET)
^{161}Tb	6.906 d	Med.	β/Auger therapy
^{166}Ho	26.80 h	Med.	β therapy
^{177}Lu	6.647 d	Med.	β therapy
^{213}Bi	45.59 m	Med.	α/β therapy
^{223}Ra	11.43 d	Med.	α therapy
^{225}Ac	10.0 d	Med.	α therapy

Ind. = nuclear industry, Med. = nuclear medicine, PET = positron emission tomography, SPECT = single photon emission computed tomography.
[a]Major release during radiological events.

2.3. Minimum detectable activity

The minimum detectable activity (MDA) was calculated for 21 radionuclides of interest (cf. Table 1). Six of these have been selected according to their relevance and occurrence in the nuclear industry (IAEA, 1998) and some of them are of major concern in the case of an accidental or malevolent release of radionuclides (NCRP, 2012). The remaining radionuclides are relevant for therapeutic applications in nuclear medicine. Some of them are already used in a clinical setting, while others have been studied for their possible applications in the field of theranostics (Cavaier et al., 2017; Ellison et al., 2015; Müller et al., 2017, 2018; Feng, 2018). Along with the therapeutic radionuclides, three of the most widespread diagnostic radionuclides (^{18}F, ^{99m}Tc and ^{68}Ga) are also considered for comparison purposes.

The MDAs were calculated with the Genie 2000 software using the ISO 11929 approach, taking into account a 5% probability of making an error of the first or second kind (i.e. $\alpha = \beta = 5\%$) (ISO, 2010). The radionuclide library used for the evaluation was updated with the Nucleonica nuclear science web portal (Nucleonica GmbH, 2017), using the JEFF-3.1 nuclear data library (Koning et al., 2006). The radionuclides half-lives were updated using the data reported in ICRP Publication 107 (ICRP, 2008). The spectra for the MDA calculation were acquired with the phantoms in the absence of sources, in a standard background environment. The spectra were measured for different acquisition times: 30, 45, 60, 120, 300, 600, 900, 1200 and 1800 s. The resulting MDAs for each radionuclide of interest were then plotted according to the inverse square root of the acquisition time. By doing so, the MDA data could be fitted to a linear function, according to its theoretically predicted behaviour (Demir et al., 2013; Gilmore, 2008).

2.4. Biokinetic models and minimum committed effective dose

The MDA fitting results were used to calculate the minimum detectable committed effective dose (MDED, in Sv) associated to an in vivo screening measurement, according to Eq. (3) :

$$MDED = MDA(t) \cdot \frac{e(50)}{m(T)} \tag{3}$$

where *MDA(t)* (in Bq) is the minimum detectable activity for a given acquisition time t, $e(50)$ (in Sv/Bq) is the committed effective dose per intake that depends on the considered route of intake (e.g. inhalation, ingestion, injection) (ICRP, 1994a, 2015, 2016, 2017) and $m(T)$ is the retention function of the considered body compartment at the elapsed time T between the intake and the measurement. It should be noted that the time of possible intake at CERN is generally known: it can be related to a specific manipulation (e.g. sample transfer and radiochemistry) or to a possible handling incident/equipment malfunctioning (e.g. dropping of the sample, ventilation failure). Occupational monitoring in these conditions is therefore task-related (ISO, 2006).

The MDED values can be used by the local radiation protection experts to estimate the maximum committed effective dose that remains undetected after a given operation. They can then limit the number of authorised operations for each worker so that the sum of all the possibly undetected committed effective doses during the year does not exceed the limit of 1 mSv.

During a screening measurement, the instrument should be placed on the body region presenting the highest retention at time T, in order to maximise the chances to detect a possible intake. In the present study, only the retention in the lungs and in the alimentary tract are applicable, due to the type of phantoms and source filling geometries considered. The retention functions $m(T)$ were taken from the Dose and Risk Calculation (DCAL) software by the Oak Ridge National Laboratory (Eckerman et al., 2006) and the OIR Data Viewer software by (ICRP, 2019b).

The DCAL software is based on the following ICRP publications: ICRP Publication 66 for the human respiratory tract model (ICRP, 1994b), ICRP Publication 30 for the gastrointestinal tract model (ICRP, 1979), ICRP Publication 68 for the dose coefficients and absorption parameter values (ICRP, 1994a), ICRP Publication 107 for the nuclear decay data (ICRP, 2008). The retention in the lungs was obtained by summing all the retention functions in the bronchioles (bb compartment), bronchi (BB compartment), thoracic lymph nodes (LN_{TH} compartment) and alveolar-interstitial region (AI compartment). The retention in the alimentary tract was obtained by summing all the retention functions in the stomach (St compartment), small intestine (SI compartment), upper large intestine (ULI compartment), and lower large intestine (LLI compartment). For both lungs and alimentary tract retention, the activity retained in the blood was distributed within the considered compartment according to the values reported in ICRP Publication 89 (ICRP, 2002; Dewji et al., 2013). By doing so, the above-described approach used to compute the retention functions using DCAL is consistent with the one adopted in the ICRP OIR Data Viewer software.

The ICRP OIR Data Viewer software is based on the following ICRP publications: ICRP Publication 130 for the human respiratory tract model (ICRP, 2015), ICRP Publication 100 for the human alimentary tract model (ICRP, 2006) and ICRP Publication 107 for the nuclear decay data (ICRP, 2008). The systemic models, the dose coefficients and the absorption parameter values are provided in the ICPR OIR report series (ICRP, 2015, 2016, 2017, 2019a).

The OIR Data Viewer software was used to obtain the values of the retention functions for the elements that have already been considered in the ICRP OIR report series. Elsewise, retention functions were provided by the DCAL software. The retention functions were computed for an adult worker, using the default particle size distribution (AMAD = 5 μm) and considering the default absorption type (S, M or F) for each radionuclide.

3. Results

3.1. Efficiency calibration

Table 2 summarises the coefficients of the efficiency curves for the two spectrometers in the different calibration geometries. The parameters are applicable for energies higher than 80 keV, corresponding to the first experimental energy-efficiency pair used for the efficiency calibration. The plots displaying the experimental efficiency data and the parametrised efficiency curves for the two spectrometers in all the considered geometries are provided in the Supplementary Material (Figures S.1 and S.2).

The efficiency calibration for the NaI(Tl) detector with the IGOR phantom in the abdomen-deep configuration was not practically feasible, even after several hours of acquisition. This was due to a combination of the low activity of the sources, the gamma radiation attenuation within the phantom itself in this geometry and the limited energy resolution of the NaI(Tl) detector. The values for this configuration are thus not reported herein.

The efficiency calibrations were validated by analysing spectra acquired with the ^{133}Ba, ^{137}Cs and ^{60}Co sources. In the case of the torso phantom, the reference sources activity ranged between 100 and 400 kBq. A 45 second-long measurement was sufficient to obtain relative differences between measured and known activities below ±5%. In the case of the IGOR phantom, we were restricted to the provided sources with relatively low activity, $1.8-34$ kBq. A 10 minutes-long acquisition was required to measure an activity within ±10% of the reference activity.

3.2. Minimum detectable activity (MDA) and minimum detectable committed effective dose (MDED)

The parameters of the MDA linear fit with respect to the inverse square root of the acquisition time are provided in Table 3 for the four sources used during the efficiency calibration. The parameters of the MDA for all the radionuclides considered in Table 1, as well as the R^2 of the fits, are provided in the Supplementary Material (Tables S.1 - S.21).

The values of the MDA calculated for an acquisition time of 30 s were used to compute the MDED according to Eq. (3). In this example, we assumed that the intake of the radionuclide of interest took place by inhalation, which is considered to be the most probable route of intake in the case of occupational exposure (Castellani et al., 2013; ICRP, 2015; ISO, 2016). As a pragmatic example, it is considered that the screening measurement is performed at the end of the working day, at $T \approx 6$ h. It should be noted that for the biokinetic models solved using DCAL, the retention is defined at $T = 6$ h and 15 min, while in the case of the OIR Data Viewer it is defined at $T = 6$ h.

The results for the Falcon 5000 and the NaI(Tl) detector are given in Tables 4 and 5, respectively. The tables show the absorption type and the committed effective dose coefficients for the corresponding radionuclides, the software used to solve the biokinetic models, the maximum value of the retention function $m(T = 6\text{h})$, the value of *MDA(t=30s)*, as well as the calculated MDED for both the torso phantom and the IGOR phantom. The values corresponding to an intake by ingestion are reported in the Supplementary Material (Tables S.22 and S.23). In the case of the IGOR phantom, the MDAs were calculated for the shallow source distribution, that was considered more anatomically realistic than the deep source distribution.

4. Discussion

4.1. Efficiency calibration

Among the efficiency curves reported in Table 2, the highest efficiency is obtained with the NaI(Tl) detector in the thorax-shallow configuration, that leads to the smallest possible distance between the sources and the instrument. For instance, the efficiency for the 80 keV peak of ^{133}Ba is 2.4 times higher than the one obtained in the same configuration for the Falcon 5000. This is due to the intrinsically higher efficiency of the NaI(Tl) crystal compared to the one of the HPGe, despite the bigger crystal volume of the latter. For the Falcon 5000, the

Table 2
Coefficients of the efficiency curves for the Falcon 5000 and the NaI(Tl) detector for the considered calibration geometries.

Instrument	Ph.	Fill.	Depth	Eq.	x_0	x_1	x_2	x_3	x_4	x_5
Falcon 5000	IGOR	TH	Deep	(2a)	−9.621E+01	5.627E+01	−1.299E+01	1.301E+00	−4.819E−02	–
Falcon 5000	IGOR	TH	Shallow	(2a)	−6.538E+01	3.666E+01	−8.136E+00	7.711E−01	−2.676E−02	–
Falcon 5000	IGOR	AB	Deep	(2a)	3.307E+02	−2.986E+02	1.037E+02	−1.773E+01	1.494E+00	−4.965E−02
Falcon 5000	IGOR	AB	Shallow	(2a)	−7.341E+01	4.031E+01	−8.790E+00	8.151E−01	−2.732E−02	–
Falcon 5000	Torso	–	–	(2b)	−1.340E−04	−3.534E+00	8.236E+01	−1.960E+03	−4.457E+05	–
NaI(Tl)	IGOR	TH	Deep	(2b)	−1.420E−04	−3.282E+00	1.703E+02	−1.097E+04	–	–
NaI(Tl)	IGOR	TH	Shallow	(2b)	−3.290E−04	−2.595E+00	9.379E+01	−4.755E+03	–	–
NaI(Tl)	IGOR	AB	Shallow	(2a)	−9.529E+00	1.583E+00	−9.861E−02	−3.137E−02	2.695E−03	–
NaI(Tl)	Torso	–	–	(2b)	−2.700E−04	−3.147E+00	7.543E+01	−6.337E+03	–	–

Ph. = phantom, Fill. = source filling geometry, TH = thorax, AB = abdomen.

Table 3
Coefficients of the MDA linear fit (MDA = $a + b \cdot x$, where $x = 1/\sqrt{t}$) for the reference radionuclides used in the calibration. The MDA is expressed in kBq and the acquisition time t in seconds.

Instrument	Ph.	Fill.	Depth	^{133}Ba		^{137}Cs		^{60}Co		^{152}Eu	
				a	b	a	b	a	b	a	b
Falcon 5000	IGOR	TH	Deep	−9.113E−03	9.694E+00	−9.268E−03	6.128E+00	−7.257E−03	4.319E+00	−1.077E−01	2.126E+01
Falcon 5000	IGOR	TH	Shallow	−3.022E−03	3.215E+00	−3.387E−03	2.239E+00	−2.707E−03	1.819E+00	−3.103E−02	7.077E+00
Falcon 5000	IGOR	AB	Deep	−2.277E−02	2.422E+01	−2.135E−02	1.412E+01	−1.653E−02	8.698E+00	−4.123E−01	5.056E+01
Falcon 5000	IGOR	AB	Shallow	−7.278E−03	7.898E+00	−7.865E−03	5.216E+00	−6.428E−03	3.787E+00	−8.981E−02	1.749E+01
Falcon 5000	Torso	–	–	−4.088E−02	1.573E+01	−3.407E−02	9.011E+00	−1.144E−03	6.350E+00	−2.652E−02	2.650E+01
NaI(Tl)	IGOR	TH	Deep	−5.009E−03	2.804E+01	−2.161E−02	2.004E+01	−7.835E−03	1.770E+01	−5.657E−02	4.988E+01
NaI(Tl)	IGOR	TH	Shallow	−2.218E−03	9.856E+00	−7.707E−03	6.928E+00	−2.756E−03	6.925E+00	−7.788E−03	1.765E+01
NaI(Tl)	IGOR	AB	Shallow	−6.314E−03	2.850E+01	−2.154E−02	1.947E+01	−7.654E−03	1.761E+01	−2.802E−02	5.946E+01
NaI(Tl)	Torso	–	–	−2.543E−02	3.898E+01	−2.836E−02	2.423E+01	−1.798E−02	2.213E+01	−3.970E−02	9.184E+01

Table 4
Falcon 5000 internal monitoring results for a single screening measurement performed 6 h after the suspected intake by inhalation, for a measurement duration of 30 s. The maximum retention is reached in the abdomen, unless stated otherwise. Configuration considered for the IGOR phantom: abdomen-shallow.

Radionuclide [–]	Abs. type [–]	$e_{50,inh}$ [Sv/Bq]	Software [–]	m(T) [–]	MDA_{IGOR} [kBq]	$MDED_{IGOR}$ [mSv]	MDA_{Torso} [kBq]	$MDED_{Torso}$ [mSv]
^{54}Mn	F	1.1E−09	DCAL	1.94E−01	0.91	0.01	1.18	0.01
^{60}Co	M	6.2E−09	OIR DV	4.00E−01	0.68	0.01	1.16	0.02
^{133}Ba	M	1.6E−09	OIR DV	4.00E−01	1.43	0.01	2.83	0.01
^{137}Cs	M	5.6E−09	OIR DV	3.50E−01	0.94	0.02	1.61	0.03
^{152}Eu	M	1.8E−08	OIR DV	4.10E−01	3.10	0.14	4.81	0.21
^{131}I	F	1.7E−08	OIR DV	1.00E−01	1.04	0.18	1.70	0.29
^{18}F	M	8.9E−11	DCAL	5.40E−04[a]	0.50	0.08	0.76	0.12
^{47}Sc	S	7.3E−10	DCAL	3.85E−01	1.48	0.00	2.77	0.01
^{64}Cu	F	6.8E−11	DCAL	8.64E−02	2.72	0.00	4.13	0.00
^{67}Cu	F	1.8E−10	DCAL	1.13E−01	1.94	0.00	3.52	0.01
^{68}Ga	F	4.9E−11	DCAL	4.53E−03	0.54	0.01	0.82	0.01
^{76}As	M	9.2E−10	DCAL	4.66E−02[a]	1.62	0.03	3.33	0.07
^{77}As	M	4.2E−10	DCAL	4.93E−02[a]	62.80	0.53	124.46	1.06
^{99m}Tc	M	1.3E−11	OIR DV	1.90E−01	1.26	0.00	2.17	0.00
^{149}Tb	M	2.9E−09	OIR DV	1.50E−01	3.14	0.06	5.62	0.11
^{161}Tb	M	3.3E−10	OIR DV	4.00E−01	18.30	0.02	92.24	0.08
^{166}Ho	M	3.5E−10	OIR DV	3.50E−01	23.13	0.02	90.10	0.09
^{177}Lu	M	2.5E−10	OIR DV	4.00E−01	9.26	0.01	16.79	0.01
^{213}Bi	M	2.9E−08	OIR DV	1.70E−03	2.95	50.33	4.55	77.68
^{223}Ra	M	1.8E−06	OIR DV	4.00E−01	6.12	27.55	12.19	54.87
^{225}Ac	F	8.9E−07	OIR DV	4.00E−01	78.71	175.13	178.13	396.34

[a]The maximum retention at $T = 6$ h is reached in the lungs. However, for the sake of simplicity, the values are reported for a measurement performed at the level of the abdomen. This allows to define a consistent, general and pragmatic measurement for all the considered radionuclides, that is thus applicable also in the case of radionuclide mixtures.

smallest efficiency is obtained with the IGOR phantom in the abdomen-deep configuration. This is due to the high attenuation caused by the empty phantom blocks that are placed between the sources and the detector (cf. Fig. 2(c)).

The calibration performed with the torso phantom leads to the second lowest efficiency for the Falcon 5000 and the lowest efficiency for the NaI(Tl) detector. This is due to the presence of 15 cm of water between the point-like source and the instruments. For both instruments, the attenuation (and thus the efficiency) for the thorax-deep configuration is similar to the one obtained in the abdomen-shallow configuration. In fact, for energies above 300 keV, the differences between the two calibration curves are smaller than 20% and 5% for the Falcon 5000 and the NaI(Tl) detector, respectively.

The efficiency calibration obtained for the Falcon 5000 and the NaI(Tl) detector in the thorax-deep configuration were compared to the ones reported by Galeev et al. (2016). The results for the Falcon 5000 are slightly higher than the published values; however, the two efficiency curves still show a good agreement, with relative differences smaller than 20%. The NaI(Tl) efficiency was compared to that of a 3”× 3” NaI(Tl) portable spectrometer characterised by Galeev et al. The efficiency of the 3”× 3” NaI(Tl) was higher than ours (with dimensions 2”× 2”) by a factor of 1.8–2.8 (depending on the energy), which is likely due to the larger crystal volume.

It should be noted that the measurements were performed without any additional shielding in order to reproduce typical screening measurement conditions and ensure the portability of the spectrometers. However, the natural background reduction provided by

Table 5
NaI(Tl) internal monitoring results for a single screening measurement performed 6 h after the suspected intake by inhalation, for a measurement duration of 30 s. The maximum retention is reached in the abdomen, unless stated otherwise. Configuration considered for the IGOR phantom: abdomen-shallow.

Radionuclide [–]	Abs. type [–]	$e_{50,inh}$ [Sv/Bq]	Software [–]	m(T) [–]	MDA_{IGOR} [kBq]	$MDED_{IGOR}$ [mSv]	MDA_{Torso} [kBq]	$MDED_{Torso}$ [mSv]
^{54}Mn	F	1.1E−09	DCAL	1.94E−01	3.18	0.02	3.89	0.02
^{60}Co	M	6.2E−09	OIR DV	4.00E−01	3.21	0.05	4.02	0.06
^{133}Ba	M	1.6E−09	OIR DV	4.00E−01	5.20	0.02	7.09	0.03
^{137}Cs	M	5.6E−09	OIR DV	3.50E−01	3.53	0.06	4.40	0.07
^{152}Eu	M	1.8E−08	OIR DV	4.10E−01	10.83	0.48	16.73	0.73
^{131}I	F	1.7E−08	OIR DV	1.00E−01	3.91	0.66	5.29	0.90
^{18}F	M	8.9E−11	DCAL	5.40E−04[a]	1.60	0.26	2.03	0.34
^{47}Sc	S	7.3E−10	DCAL	3.85E−01	4.99	0.01	7.60	0.01
^{64}Cu	F	6.8E−11	DCAL	8.64E−02	8.70	0.01	11.09	0.01
^{67}Cu	F	1.8E−10	DCAL	1.13E−01	7.10	0.01	10.33	0.02
^{68}Ga	F	4.9E−11	DCAL	4.53E−03	1.73	0.02	2.20	0.02
^{76}As	M	9.2E−10	DCAL	4.66E−02[a]	7.00	0.14	8.79	0.17
^{77}As	M	4.2E−10	DCAL	4.93E−02[a]	231.36	1.97	337.39	2.87
^{99m}Tc	M	1.3E−11	OIR DV	1.90E−01	3.62	0.00	5.74	0.00
^{149}Tb	M	2.9E−09	OIR DV	1.50E−01	10.89	0.21	14.80	0.29
^{161}Tb	M	3.3E−10	OIR DV	4.00E−01	23.09	0.02	87.28	0.07
^{166}Ho	M	3.5E−10	OIR DV	3.50E−01	34.66	0.03	106.09	0.11
^{177}Lu	M	2.5E−10	OIR DV	4.00E−01	33.83	0.02	48.63	0.03
^{213}Bi	M	2.9E−08	OIR DV	1.70E−03	11.74	200.31	15.32	261.37
^{223}Ra	M	1.8E−06	OIR DV	4.00E−01	9.44	42.48	26.41	118.85
^{225}Ac	F	8.9E−07	OIR DV	4.00E−01	140.66	312.98	351.30	781.63

[a]The maximum retention at $T = 6$ h is reached in the lungs. However, for the sake of simplicity, the values are reported for a measurement performed at the level of the abdomen. This allows to define a consistent, general and pragmatic measurement for all the considered radionuclides, that is thus applicable also in the case of radionuclide mixtures.

shielding allows to achieve lower MDA, especially for radionuclides emitting (mainly) photons with energies below 150 keV and may thus be considered to improve the detection performance for such radioisotopes.

4.2. Minimum detectable activity (MDA)

The low instrument efficiency obtained with the torso and with the IGOR phantoms in the abdomen-deep configuration directly translates in higher MDAs.

The obtained MDA values were compared to the ones published in the literature for some among the most commonly-encountered radionuclides. Galeev et al. report MDA results of 1.4 kBq for ^{137}Cs and 1.2 kBq for ^{60}Co for a 60 s measurement done using the Falcon 5000 and the IGOR phantom in the thorax-deep configuration (Galeev et al., 2016). These values are approximately a factor of two higher than the ones obtained in our study for the same acquisition time (0.8 kBq for ^{137}Cs and 0.6 kBq for ^{60}Co, respectively). Galeev et al. calculated the detection limits according to the ISO 11929 standard, but considered an additional user-defined source of uncertainty resulting from a different approach to estimate the net peak area uncertainty. This involved the use of other spectral analysis software packages in addition to the Genie 2000 software provided by the Falcon 5000 manufacturer. Their approach thus leads to higher MDA values than the ones directly provided by the Genie 2000 software used in our work and that are likely to be adopted by a general Falcon 5000 user.

Another study reports an MDA of approximately 1.3 kBq for ^{137}Cs using a 3"× 3" NaI detector and an acquisition time of 60 s (Ha and Kim, 2016). The instrument was calibrated for a whole-body geometry using the reference male Bottle Mannequin Absorber (BOMAB) phantom (ANSI, 1999). The MDA values that we obtain in our study for the same acquisition time using the 2"× 2" NaI(Tl) detector are generally higher (2.6 kBq for the IGOR phantom and thorax-deep configuration, 2.5 kBq for the IGOR phantom and abdomen-shallow configuration, 3 kBq for the torso phantom), with exception of the IGOR phantom and thorax-shallow configuration (0.9 kBq). These differences can be explained by multiple factors, including: the use of different phantoms (BOMAB, IGOR, torso phantom), the detector size and its positioning with respect to the phantoms, the background at the time of the measurements, the approach used to calculate the MDA. Despite these differences, the results are in the same order of magnitude with a maximum difference of a factor of 2.3.

Another study featured an in-house developed phantom consisting of three 5000 cm^3 bags uniformly contaminated with ^{18}F and ^{99m}Tc that were placed in a plastic drum (Terranova et al., 2010). The MDAs were determined using the Currie's approach for a 1.5" × 2.2" NaI(Tl) inserted between the bags and an acquisition time of 300 s. The reported MDAs for the two radionuclides varied between 200–400 Bq. The results found in this study were in the range of 200–1100 for measurements performed with the IGOR phantom in all available configurations.

Considering the great variability occurring between the reported results in occupational radiation protection studies, it possible to state that the MDA values obtained in this work show a good agreement with the previously published results, despite the different phantom geometries and MDA calculation approaches.

4.3. Minimum committed effective dose (MDED)

Six hours after the intake, the retention functions of nearly all the radionuclides considered in this study reach their maximum values in the alimentary tract. The exceptions are ^{18}F, ^{76}As and ^{77}As, for which the retention is 11 (fluorine) and 1.6 (arsenic) times higher in the lungs than in the alimentary tract. Among these radionuclides, ^{77}As is of major concern as it presents MDED values that can exceed the dose limit of 1 mSv after a single measurement. If needed, its MDED can be reduced by up to a factor of 5 when measuring at the level of the lungs. Therefore, if only ^{18}F, ^{76}As and ^{77}As are at risk of inhalation, we suggest placing the instruments at the level of the lungs to reduce the MDED values.

It should be noted that for the examples provided in Tables 4 and 5, the MDA and MDED were calculated considering the shortest acquisition time available in this study (30 s). However, the data from Tables S.1-S.21 provided in the Supplementary Material allow the assessment of the MDA for longer measuring times (up to 30 min). As stated in the previous paragraphs, the MDA shows a linear correlation with the square root of the acquisition time. As a first approximation, the value of the MDA (and thus that of the MDED) is halved when increasing the acquisition time by a factor of 4. Alternatively, it is possible to use Eq. (3) to calculate the MDA associated to a defined

MDED value and use the information provided in the Supplementary Material to obtain the corresponding acquisition time.

The suggested approach is not directly applicable to ^{213}Bi, ^{223}Ra and ^{225}Ac, since the calculated MDEDs after a single operation are significantly above 1 mSv. In the case of ^{213}Bi, this is mainly due to its short half-life that results in a small retention in the considered compartments after 6 h. To overcome this limitation, the elapsed time between the intake and the measurement needs to be reduced. For instance, a 30 s measurement performed 1 h after the intake leads to an MDED of 0.78 mSv (Falcon 5000 measuring in the IGOR abdomen-shallow configuration). In the case of ^{223}Ra and ^{225}Ac, the high MDEDs are mainly due to a combination of their significant $e(50)$ coefficients (α-emitters) and their high MDA values caused by low photonic emission probabilities. The MDED for ^{223}Ra can be reduced to ≈ 3 mSv when performing a 30 minutes-long measurement (Falcon 5000 measuring in the IGOR abdomen-shallow configuration), while the MDED for ^{225}Ac cannot be reduced below 22 mSv for the same configuration and acquisition time. A rapid in vivo approach like the one suggested in this work is thus not suitable for the occupational monitoring of these two radionuclides, for which in vitro measurements need to be considered (Saurat et al., 2018).

4.4. Limitations of the study

This study has three main limitations.

First, the elapsed time between the suspected intake and the screening measurement should be carefully respected. The retention functions may present significant changes according to time, especially for short-lived isotopes such as ^{18}F, ^{68}Ga and ^{213}Bi. Therefore, this may greatly impact the MDED if the measuring interval is not respected or if the moment of the suspected intake is not precisely known. For instance, if the time of suspected intake is misidentified and takes place 1 h before the in vivo measurement, the values presented in Tables 4 and 5 may over or underestimate the actual MDED ($MDED_{T=6h}/MDED_{T=1h}$ varying between 0.7 and 4.4, without taking into account the short-lived radionuclides ^{18}F, ^{68}Ga and ^{213}Bi, for which this ratio would take the values of 250, 27 and 65, respectively).

It should also be noted that even if the precise moment of the suspected intake is known, a measurement performed right after the suspected intake may provide significant MDED values due to the time needed by the incorporated radionuclide to accumulate in the considered body region. A good knowledge of the retention function for the radionuclide of interest is therefore paramount to apply the approach suggested in this study.

Second, the MDED values provided in Tables 4 and 5 are obtained by solving the biokinetic models of the considered radionuclides. For this reason, the values cannot be directly used for the internal monitoring of the radiopharmaceuticals handled in nuclear medicine, as their distribution in the body will follow the biokinetics of the attached biomolecule rather than the one of the radioelement itself (Dantas et al., 2008). The values reported in this study are thus only directly applicable for the triage monitoring of workers that may incorporate the radionuclides prior to any modification affecting their chemical characteristics and hence their biokinetics. However, the presented approach could be extended to the monitoring of the medical staff working in nuclear medicine services, provided that the biokinetics of the administered compound are known.

Third, it should be noted that the calibration spectra were acquired without placing any additional ^{40}K sources (naturally-occurring radionuclide found in the human body) in the phantoms. One of the purposes of the work was to compare the instruments response obtained with the torso and IGOR phantoms. Since no ^{40}K sources were available for the simplified torso phantom, the IGOR phantom was not equipped with ^{40}K to avoid bias in the comparison.

5. Conclusions

This study presents the approach used to characterise two portable gamma spectrometers and determine whether they can be used to monitor the internal contamination of workers and guarantee the detection of intakes leading to $E_{50} > 1$ mSv/year. In particular, we assessed their ability to detect 21 of the most commonly encountered radionuclides in the nuclear industry along with novel radioisotopes that are being considered for promising applications in therapeutic nuclear medicine, for which an internal dosimetry monitoring programme is not yet established. We characterised the spectrometers efficiencies using two phantoms: a simplified, easily reproducible model of the torso and a widely used anthropomorphic phantom. We considered different activity distributions within the phantoms in order to simulate activity retention in the lungs and in the alimentary tract. The minimum detectable activity was calculated and parametrised for different acquisition times, ranging from 30 s to 30 min. Biokinetic models and committed effective dose coefficients were used to estimate the minimum detectable committed effective dose as a function of the acquisition time and the interval elapsed between the intake and the measurement. The results show that the efficiency obtained with the simplified torso phantom is generally the most conservative and can thus be used for a pragmatic, cost-effective and safe approach. For an acquisition time of 30 s and a single measurement performed 6 h after the possible intake, the minimum detectable committed effective doses range between few tens up to hundreds of μSv (with the exception of three α-emitting radionuclides presenting minimum doses exceeding 1 mSv). This work shows that the monitoring of internal contamination using portable spectrometers is indeed feasible not only in the case of radiological emergencies involving common radionuclides, but also for rapid routine monitoring of occupationally exposed workers handling novel radioisotopes.

Declaration of competing interest

The authors declare that they have no known competing financial interests or personal relationships that could have appeared to influence the work reported in this paper.

Acknowledgements

The authors would like to thank Frank Assenmacher, Roman Galeev and their colleagues from the Division for Radiation Safety and Security at the Paul Scherrer Institut (Villigen, Switzerland) for kindly lending the IGOR phantom and its sources. The authors are also grateful to the colleagues of the Institute of Radiation Physics in Lausanne: Thierry Buchillier for his precious advices concerning spectroscopy analysis, Corinne Moratal for her know-how concerning the manufacturing of the IGOR sources and Silvano Gnesin and Marietta Straub for their help in selecting the relevant radionuclides for our study. Special thanks go to Nicolas Riggaz from the Radiation Protection Group at CERN for his technical assistance concerning the use of the Genie 2000 software.

Appendix A. Supplementary data

Supplementary material related to this article can be found online at https://doi.org/10.1016/j.radmeas.2020.106426.

References

ANSI, 1999. Specifications for the Bottle Manikin Absorption Phantom. ANSI/HPS, (N13.35), American National Standard Institute/Health Phyiscs Society, McLean.

Castellani, C., Marsh, J., Hurtgen, C., Blanchardon, E., Berard, P., Giussani, A., Lopez, M., 2013. IDEAS Guidelines (Version 2) for the Estimation of Committed Doses from Incorporation Monitoring Data. EURADOS Report, (2013–01), European Radiation Dosimetry Group, Braunschweig.

Cavaier, R.F., Haddad, F., Sounalet, T., Stora, T., Zahi, I., 2017. Terbium radionuclides for theranostics applications: A focus on MEDICIS-PROMED. Physics Procedia 90, 157–163.

Dantas, B.M., Lucena, E.A., Dantas, A.L.A., 2008. Internal exposure in nuclear medicine: Application of IAEA criteria to determine the need for internal monitoring. Braz. Arch. Biol. Technol. 51 (N.SPE), 103–107.

Demir, D., Eroğlu, M., Turşucu, A., 2013. Studying of characteristics of the HPGe detector for radioactivity measurements. J. Instrum. 8 (10), P10027.

Dewji, S., Hertel, N., Ansari, A., 2013. Assessing internal contamination after the detonation of a radiological dispersion device using a 2×2-inch sodium iodide detector. Radiat. Prot. Dosim. 155 (3), 300–316.

EC, 2018. Technical Recommendations for Monitoring Individuals for Occupational Intakes of Radionuclides. Radiation Protection Series, (No. 188), European Commission, Luxembourg.

Eckerman, K., Leggett, R., Cristy, M., Nelson, C., Ryman, J., Sjoreen, A., Ward, R., 2006. DCAL: Dose and Risk Calculation System, ver. 9.4. Oak Ridge National Laboratory, Life Science Division, Dosimetry Research Group, www.epa.gov/radiation/dcal-software-and-resources. (Accessed 6 November 2019).

Ellison, P.A., Barnhart, T.E., Chen, F., Hong, H., Zhang, Y., Theuer, C.P., Cai, W., Nickles, R.J., DeJesus, O.T., 2015. High yield production and radiochemical isolation of isotopically pure arsenic-72 and novel radioarsenic labeling strategies for the development of theranostic radiopharmaceuticals. Bioconjug. Chem. 27 (1), 179–188.

Feng, Y., 2018. Arsenic-72, 77 as a Matched Pair Radiopharmaceutical for Imaging and Radiotherapy (Ph.D. thesis). University of Missouri-Columbia.

FOPH, 2017a. Ordonnance du DFI sur la dosimétrie individuelle et la dosimétrie de l'environnement (Ordonnance sur la dosimétrie), du 26 avril 2017. RS, (814.501.43), Federal Office of Public Health, Bern.

FOPH, 2017b. Ordonnance sur la radioprotection (ORaP), du 26 avril 2017. RS, (814.501), Federal Office of Public Health, Bern.

Galeev, R., Butterweck, G., Boschung, M., Hofstetter-Boillat, B., Hohmann, E., Mayer, S., 2016. Suitability of portable radionuclide identifiers for emergency incorporation monitoring. Radiat. Prot. Dosim. 173 (1–3), 145–150.

Gilmore, G.R., 2008. Practical Gamma-ray Spectrometry, second ed. John Wiley & Sons, Ltd, ISBN: 9780470861981, p. 252, chapter 13.

Ha, W.-H., Kim, J.K., 2016. Optimization of in-vivo monitoring program for radiation emergency response. J. Radiat. Prot. Res. 41 (4), 333–338.

IAEA, 1998. Radiological Characterization of Shut Down Nuclear Reactors for Decommissioning Purposes. IAEA Technical Reports Series, (No. 389), International Atomic Energy Agency, Vienna.

IAEA, 1999. Assessment of occupational exposure due to intake of radionuclides. IAEA Safety Standard Series, (No. RS-G-1.2), International Atomic Energy Agency, Vienna.

ICRP, 1979. Limits for intakes of radionuclides by workers. ICRP publication 30 (part 1). Ann. ICRP, (2(3-4)), International Commission on Radiological Protection.

ICRP, 1994a. Dose Coefficients for Intakes of Radionuclides by Workers. ICRP Publication 68. Ann. ICRP, (24(4)), International Commission on Radiological Protection.

ICRP, 1994b. Human Respiratory Tract Model for Radiological Protection. ICRP Publication 66. Ann. ICRP, (24(1-3)), International Commission on Radiological Protection.

ICRP, 2002. Basic anatomical and physiological data for use in radiological protection reference values. ICRP publication 89. Ann. ICRP, (32 (3-4)), International Commission on Radiological Protection.

ICRP, 2006. Human Alimentary Tract Model for Radiological Protection. ICRP Publication 100. Ann. ICRP, (36 (1-2)), International Commission on Radiological Protection.

ICRP, 2008. Nuclear Decay Data for Dosimetric Calculations. Ann. ICRP, (38(3)), International Commission on Radiological Protection.

ICRP, 2015. Occupational Intakes of Radionuclides: Part 1. ICRP Publication 130. Ann. ICRP, (44(2)), International Commission on Radiological Protection.

ICRP, 2016. Occupational Intakes of Radionuclides: Part 2. ICRP Publication 134. Ann. ICRP, (45(3/4)), International Commission on Radiological Protection.

ICRP, 2017. Occupational Intakes of Radionuclides: Part 3. ICRP Publication 137. Ann. ICRP, (46(3/4)), International Commission on Radiological Protection.

ICRP, 2019a. Occupational Intakes of Radionuclides: Part 4. ICRP Publication 141. Ann. ICRP, (48(2/3)), International Commission on Radiological Protection.

ICRP, 2019b. OIR Data Viewer Electronic Annex, Ver. 4.01.04.19. International Commission on Radiological Protection, https://journals.sagepub.com/doi/suppl/10.1177/ANIB_48_2-3/suppl_file/. (Accessed 15 January 2020).

ICRU, 2003. Direct Determination of the Body Content of Radionuclides. ICRU Report, (69. J. ICRU 3 (1)), International Commission on Radiation Units and Measurement, Bethesda.

ISO, 2006. Radiation Protection – Monitoring of Workers Occupationally Exposed to a Risk of Internal Contamination with Radioactive Material. ISO, (20553:2006), International Organization for Standardization, Geneva.

ISO, 2010. Determination of the Characteristic Limits (Decision Threshold, Detection Limit and Limits of the Confidence Interval) for Measurements of Ionizing Radiation – Fundamentals and Application. ISO, (11929:2010), International Organization for Standardization, Geneva.

ISO, 2011. Radiation Protection – Dose Assessment for the Monitoring of Workers for Internal Radiation Exposure. ISO, (27048:2011), International Organization for Standardization, Geneva.

ISO, 2016. Radiation Protection – Monitoring and Internal Dosimetry for Staff Members Exposed to Medical Radionuclides as Unsealed Sources. ISO, (16637:2016), International Organization for Standardization, Geneva.

Koning, A., Forrest, R., Kellett, M., Mills, R., Henriksson, H., Rugama, Y., Bersillon, O., Bouland, O., Courcelle, A., Duijvestijn, M., et al., 2006. The JEFF-3.1 nuclear data library - JEFF Report 21. NEA, (No. 6190), Nuclear Energy Agency.

Kovtun, A., Firsanov, V., Fominykh, V., Isaakyan, G., 2000. Metrological parameters of the unified calibration whole-body phantom with gamma-emitting radionuclides. Radiat. Prot. Dosim. 89 (3–4), 239–242.

Kramer, G., Capello, K., Hauck, B., 2005. The HML's new field deployable, high-resolution whole body counter. Health. Phys. 89 (5), 60–68.

KSR, 2001a. Ganzkörper - und Schilddrüsenmessplätze - Empfehlungen zur Standardisierung der Kalibrierung. Technical Report, Swiss Expert Group for Personal Dosimetry - Eidgenössische Kommission für Strahlenschutz und Überwachung der Radioaktivität.

KSR, 2001b. Thoraxmessplätze für Triagemessung - Empfehlungen zur Standardisierung der Kalibrierung und Prüfung . Technical Report, Swiss Expert Group for Personal Dosimetry - Eidgenössische Kommission für Strahlenschutz und Überwachung der Radioaktivität.

Medici, S., Carbonez, P., Damet, J., Bochud, F., Bailat, C., Pitzschke, A., 2019. Detecting intake of radionuclides: In vivo screening measurements with conventional radiation protection instruments. Radiat. Meas. 122, 126–132.

Muikku, M., Rahola, T., 2007. Improvement of the measuring equipment used in the assessment of internal doses in emergency situations. Radiat. Prot. Dosim. 127 (1–4), 277–281.

Müller, C., Domnanich, K.A., Umbricht, C.A., van der Meulen, N.P., 2018. Scandium and terbium radionuclides for radiotheranostics: Current state of development towards clinical application. Br. J. Radiol. 91 (1091), 20180074.

Müller, C., van der Meulen, N.P., Benešová, M., Schibli, R., 2017. Therapeutic radiometals beyond 177Lu and 90Y: Production and application of promising a-particle, b-particle, and auger electron emitters. J. Nucl. Med. 58 (suppl 2), 91S–96S.

NCRP, 2012. Population monitoring and radionuclide decorporation following a radiological or nuclear accident. NCRP Report, (No. 166), National Council on Radiation Protection and Measurements, Bethesda, Maryland.

Nucleonica GmbH, 2017. Nucleonica Nuclear Science Portal, Version 3.0.146.0001. Nucleonica GmbH, Karlsruhe, Germany, www.nucleonica.com. (Accessed 6 November 2019).

Saurat, D., Aupée, O., Gontier, E., Métivier, D., Cazoulat, A., Lecompte, Y., 2018. Recommendations for monitoring and internal dosimetry for nuclear medicine staff exposed to radiopharmaceuticals 223Ra dichloride. Radiat. Prot. Dosim. 182 (3), 299–309.

Terranova, N., Testoni, R., Cicoria, G., Mostacci, D., Marengo, M., 2010. Assessment of internal contamination hazard and fast monitoring for workers involved in maintenance operations on PET cyclotrons. Radiat. Prot. Dosim. 144 (1–4), 468–472.

Youngman, M., 2008. The Use of a High-Resolution Radionuclide Identifier as a Portable Whole Body Monitor. HPA-RPD-045, Health Protection Agency, Chilton, Didcot, Oxfordshire, UK.